HHS Public Access

Author manuscript

Gastroenterology. Author manuscript; available in PMC 2024 May 01.

Published in final edited form as:

Gastroenterology. 2024 May ; 166(5): 772–786.e14. doi:10.1053/j.gastro.2024.01.027.

Oncogenic Fatty Acid Metabolism Rewires Energy Supply Chain in Gastric Carcinogenesis

Yoonkyung Won[1,2], **Bogun Jang**[1,2,3], **Su-Hyung Lee**[1,2], **Michelle L. Reyzer**[4], **Kimberly S. Presentation**[1,2], **Hyesung Kim**[1,2,5], **Brianna Caldwell**[1,2], **Changqing Zhang**[1,2], **Hye Seung Lee**[6,7], **Cheol Lee**[7], **Vincent Q. Trinh**[8], **Marcus C. B. Tan**[1,2,9], **Kwangho Kim**[10,11], **Richard M. Caprioli**[4], **Eunyoung Choi**[1,2,12]

[1]Department of Surgery, Vanderbilt University Medical Center, Nashville, Tennessee

[2]Epithelial Biology Center, Vanderbilt University Medical Center, Nashville, Tennessee

[3]Department of Pathology, Jeju National University College of Medicine and Jeju National University Hospital, Jeju, Republic of Korea

[4]Mass Spectrometry Research Center, Vanderbilt University, Nashville, Tennessee

[5]Department of Pathology, Jeju National University College of Medicine, Jeju, Republic of Korea

Correspondence Address correspondence to: Eunyoung Choi, PhD, Department of Surgery and Epithelial Biology Center, Vanderbilt University Medical Center, MRB IV 10435F, 2213 Garland Avenue, Nashville, Tennessee 37232. eunyoung.choi@vumc.org.
Author names in bold designate shared co-first authorship.

CRediT Authorship Contributions

Yoonkyung Won, PhD (Conceptualization: Lead; Data curation: Lead; Formal analysis: Lead; Investigation: Lead; Methodology: Lead; Visualization: Lead; Writing – original draft: Lead; Writing – review & editing: Supporting)
Bogun Jang, MD, PhD (Formal analysis: Supporting; Funding acquisition: Supporting; Investigation: Supporting; Methodology: Supporting; Validation: Supporting; Visualization: Supporting; Writing – original draft: Supporting; Writing – review & editing: Supporting)
Su-Hyung Lee, DVM, PhD (Data curation: Supporting; Investigation: Supporting; Methodology: Supporting; Validation: Supporting; Visualization: Supporting; Writing – original draft: Supporting; Writing – review & editing: Supporting)
Michelle L. Reyzer, PhD (Formal analysis: Supporting; Investigation: Supporting; Methodology: Supporting; Validation: Supporting; Writing – original draft: Supporting; Writing – review & editing: Supporting)
Kimberly S. Presentation, BS (Investigation: Supporting; Methodology: Supporting; Validation: Supporting)
Hyesung Kim, PhD (Formal analysis: Supporting; Investigation: Supporting; Methodology: Supporting; Validation: Supporting; Writing – review & editing: Supporting)
Brianna Caldwell, MS (Methodology: Supporting; Writing – review & editing: Supporting)
Changqing Zhang, BS (Methodology: Supporting; Validation: Supporting)
Hye Seung Lee, MD (Resources: Supporting)
Cheol Lee, MD (Resources: Supporting)
Vincent Q. Trinh, MD (Resources: Supporting; Writing – review & editing: Supporting)
Marcus C.B. Tan, MD (Funding acquisition: Supporting; Resources: Supporting; Writing – review & editing: Supporting)
Kwangho Kim, PhD (Formal analysis: Supporting; Investigation: Supporting; Methodology: Supporting; Software: Supporting; Validation: Supporting; Visualization: Supporting)
Richard M. Caprioli, PhD (Resources: Supporting)
Eunyoung Choi, PhD (Conceptualization: Lead; Data curation: Supporting; Funding acquisition: Lead; Project administration: Lead; Resources: Lead; Supervision: Lead; Visualization: Supporting; Writing – original draft: Lead; Writing – review & editing: Lead)

Conflicts of interest

The authors disclose no conflicts.

Supplementary Material

Note: To access the supplementary material accompanying this article, visit the online version of *Gastroenterology* at www.gastrojournal.org, and at https://doi.org/10.1053/j.gastro.2024.01.027.

[6]Cancer Research Institute, Seoul National University College of Medicine, Seoul, Republic of Korea

[7]Department of Pathology, Seoul National University College of Medicine, Seoul, Republic of Korea

[8]The Digital Histology and Advanced Pathology Research, The Institute for Research in Immunology and Cancer (IRIC) of the Université de Montréal, Montréal, Québec, Canada

[9]Vanderbilt Ingram Cancer Center, Vanderbilt University Medical Center, Nashville, Tennessee

[10]Vanderbilt Institute of Chemical Biology, Vanderbilt University, Nashville, Tennessee

[11]Department of Chemistry, Vanderbilt University, Nashville, Tennessee

[12]Department of Cell and Developmental Biology, Vanderbilt University, Nashville, Tennessee

Abstract

BACKGROUND & AIMS: Gastric carcinogenesis develops within a sequential carcinogenic cascade from precancerous metaplasia to dysplasia and adenocarcinoma, and oncogenic gene activation can drive the process. Metabolic reprogramming is considered a key mechanism for cancer cell growth and proliferation. However, how metabolic changes contribute to the progression of metaplasia to dysplasia remains unclear. We have examined metabolic dynamics during gastric carcinogenesis using a novel mouse model that induces Kras activation in zymogen-secreting chief cells.

METHODS: We generated a *Gif-rtTA;TetO-Cre;Kras*^{G12D} (GCK) mouse model that continuously induces active Kras expression in chief cells after doxycycline treatment. Histologic examination and imaging mass spectrometry were performed in the GCK mouse stomachs at 2 to 14 weeks after doxycycline treatment. Mouse and human gastric organoids were used for metabolic enzyme inhibitor treatment. The GCK mice were treated with a stearoyl- coenzyme A desaturase (SCD) inhibitor to inhibit the fatty acid desaturation. Tissue microarrays were used to assess the SCD expression in human gastrointestinal cancers.

RESULTS: The GCK mice developed metaplasia and high-grade dysplasia within 4 months. Metabolic reprogramming from glycolysis to fatty acid metabolism occurred during metaplasia progression to dysplasia. Altered fatty acid desaturation through SCD produces a novel eicosenoic acid, which fuels dysplastic cell hyperproliferation and survival. The SCD inhibitor killed both mouse and human dysplastic organoids and selectively targeted dysplastic cells in vivo. SCD was up-regulated during carcinogenesis in human gastrointestinal cancers.

CONCLUSIONS: Active Kras expression only in gastric chief cells drives the full spectrum of gastric carcinogenesis. Also, oncogenic metabolic rewiring is an essential adaptation for high-energy demand in dysplastic cells.

Keywords

Carcinogenesis; Fatty Acid Metabolism; Kras; Imaging Mass Spectrometry; Stearoyl-CoA Desaturase

Gastrointestinal cancers are common life-threatening cancers and occur along the digestive tract epithelium, including the esophagus, stomach, and pancreas.[1] Evolution of epithelial cancers involves a multistep carcinogenic process from precancerous metaplasia to dysplasia and adenocarcinoma involving alterations of genetic, epigenetic, and metabolic pathways.[2–4] Carcinogenesis often requires oncogenic gene activation, which initiates signaling pathways, including the RAS signaling pathway. In the stomach, metaplasia arises from zymogen-secreting chief cell plasticity in response to severe gastric injury, which is potentially reversible.[5–7] However, cell plasticity also permits the entry of metaplastic cells into a carcinogenic process, leading to dysplasia and adenocarcinoma.[8] Also, previous studies have noted that Kras activation and amplification can lead to gastric carcinogenesis.[9–12]

Gastric dysplasia is the focal neoplastic lesion that has the highest risk of cancer development. Dysplasia is generally recognized by histologic features, such as changes in nucleus and cytoplasm in cells.[13,14] Our group recently identified a stem cell population that is first present in the dysplastic stage and displays tumorigenic capacity.[13] However, molecular and cellular mechanisms of precancerous metaplasia progression to dysplasia and even to adenocarcinoma still remain poorly understood.

Metabolism includes chemical reactions for cell homeostasis, energy production, or generation of biological building blocks in cells. Cells often stabilize or switch metabolic pathways to control signaling pathways. Recent studies have reported that bioactive metabolites, such as fatty acids (FAs), can regulate cellular heterogeneity, tumor growth, and immune response.[15–18] FAs are an essential element for a variety of biological processes, including energy supply and storage, cell signaling, transcription control, phospholipid synthesis, and membrane fluidity.[19] Also, FA metabolism is associated with tumor progression, metastasis, and drug resistance in cancer.[19–21] However, whether FA metabolism occurs during early stages of carcinogenesis or even whether any specific metabolic pathways can regulate the process remains unidentified.

In this study, we used a novel mouse model that induces Kras activation in zymogen-secreting chief cells leading to the development of high-grade dysplasia (HGD) in mouse stomachs. We performed imaging mass spectrometry (IMS) using the Kras-induced stomach tissues to examine dynamic changes in metabolites during carcinogenic transition of metaplasia to dysplasia. We identified an altered FA metabolic pathway that produces a novel eicosenoic acid (EA) as a major energy source required for dysplastic cell proliferation and survival.

Materials and Methods

Mice and Drug Treatment

All mice experiments in this study followed protocols approved by the Vanderbilt University Medical Center Institutional Animal Care and Use Committees.

Littermates or age-matched mice were randomly allocated to experimental or control groups. To generate the *Gif-rtTA;TetO-Cre;Kras*^{G12D} (GCK) mice, the *Gif-rtTA* mice were crossed with *TetO-Cre* mice and *Lox-Stop-Lox (LSL)-Kras*^{G12D} mice (no. 006234 and 008179, The

Jackson Laboratories). For the induction of Cre-mediated recombination, 6-week-old mice were administered with water containing doxycycline at a concentration of 1 mg/mL for 2 weeks. Mice were humanely killed between 2 to 14 weeks after doxycycline treatment for histologic examination. A939572 (HY-50709; MedChemExpress) was dissolved in dimethyl sulfoxide as a 100 mg/mL stock. The GCK mice were administered A939572 daily for 2 weeks by intraperitoneal injection (20 mg/kg diluted in corn oil) at 6 weeks after doxycycline treatment.

Organoid Culture and Treatment

Mouse gastric organoids were established from corpus mucosa in untreated or GCK mouse stomachs as described previously.[22] Gastric organoids were passaged and cultured in ECM Gel (E1270, Sigma-Aldrich) or Cultrex Reduced Growth Factor Basement Membrane Extract, Type R1 (3433–005-R1, R&D Systems) with Mouse IntestiCult medium (06005, STEMCELL Technologies) supplemented with 1% penicillin/streptomycin (2441832, Gibco). Human gastric organoids were previously established from patients who underwent curative gastrectomy as described[13,23] and cultured in Corning Matrigel Membrane Matrix (356231, Thermo Fisher Scientific) with Human IntestiCult medium (06010, StemCell Technology) supplemented with 1% penicillin/streptomycin, 0.2% MycoZap (VZA-2031, Lonza).

For metabolic enzyme inhibitor treatment, metabolic enzyme inhibitor-containing media was added 1 day after passaging and cultured for 3 days. Detailed information of inhibitors is provided in Supplementary Table 1. For metabolite cotreatment, media containing A939572 with either *cis*-11- EA or *cis*-7,10,13,16-docosatetraenoic acid (DA) were added 1 day after passaging and cultured for 3 days. Detailed information on metabolites is provided in Supplementary Table 1. Phase-contrast images of organoids were captured using the EVOS M7000 inverted microscope (Thermo Fisher Scientific) or the JuLI stage (NanoEntek). The JuLI stage was also used to monitor the growth and morphologic changes of the organoids in real time. Quantitative data analyses were performed using images from at least 3 replicates at 4× magnification.

For measurement of organoid growth, the diameters of organoids were manually measured from 3 entire well images of each condition at 4× magnification using the ZEN 3.3 software measuring tool. For calcein acetoxymethyl/ethidium-1 staining, organoids were transferred to microfluidic-based flow chips (Protein Fluidics). Media containing A939572 with either *cis*-11-EA or *cis*-7,10,13,16-DA was added to the organoids and cultured for 3 days. The organoids were stained with 2 μmol/L calcein acetoxymethyl and 4 μmol/L ethidium-1 (L3224, Thermo Fisher Scientific) for 30 minutes at 37° C and images were captured using a Zeiss LSM 880 using at 20× magnification. To prepare paraffin-embedded organoid sections, mouse or human gastric organoids in Matrigel were fixed in 4% paraformaldehyde for 30 minutes at room temperature and washed with 1X phosphate-buffered saline. The organoids were embedded in Epredia HistoGel (HG-4000–012, Thermo Fisher Scientific) and processed.

Imaging Mass Spectrometry

Frozen stomach tissues from the GCK mice were sectioned at 12-μm thickness and thaw-mounted onto indium-tin oxide–coated glass slides. Matrix-assisted laser desorption/ionization (MALDI) matrix 9-aminoacridine was spray-coated onto the MALDI target plates via an automatic sprayer (TM Sprayer; HTX Technologies). 9-Aminoacridine was made up as 5 mg/mL in 90% methanol, and 4 passes were used with a nozzle temperature of 85°C, a flow rate of 0.15 mL/min, 2-mm track spacing, and a stage velocity of 700 mm/min. Nitrogen was used as the nebulization gas and was set to 10-gauge pressure (psig). Images were acquired with a 15T Fourier transform ion cyclotron resonance mass spectrometer (SolariX; Bruker Daltonics) equipped with an Apollo II dual-ion source and Smartbeam II 2 kHz neodymium:yttrium-aluminum-garnet laser that was frequency tripled to a 355-nm wavelength. Data were collected in the negative ion mode with the laser operating at 2 kHz. The pixel spacing was 50 μm (center-to-center distance) in both x and y dimensions. Data were collected from mass-to-charge (m/z) ratio 100 to 1400 with a resolving power of 190,000 at m/z 300.

Tentative metabolite identifications were made by accurate mass, typically better than 1 ppm. The metabolites were identified by searching against the LIPID MAPS (Lipidomics Gateway, http://www.lipidmaps.org) and METLIN (The Scripps Research Institute, https://metlin.scripps.edu) online databases, which are reported using total carbon: double bond nomenclature. Fleximaging 5.0 (Bruker Daltonics) was used for ion image visualization and data analysis. Relative quantification was performed by exporting the pixel intensities of the pooled data segments and excluding zero-intensity values using Fleximaging 5.0 and mMass software. The relative quantification data are summarized in Supplementary Table 2.

Further detailed methods are included in the Supplementary Methods.

Results

Expression of Active Form of Kras in Gastric Chief Cells Leads to the Development of Metaplasia and High-Grade Dysplasia

To determine whether an expression of active form of Kras only in gastric chief cells can lead to the entire process of gastric carcinogenesis, we generated the novel GCK novel transgenic mouse strain, *Gif-rtTA;TetO-Cre;LSL-Kras*^{G12D} mice, by crossing the *Gif-rtTA* mice, a doxycycline-inducible and chief cell-specific driver mouse allele,[7] with the *TetO-Cre* and *LSL-Kras*^{G12D} alleles (Supplementary Figure 1A). The GCK mice developed metaplasia, followed by low-grade dysplasia (LGD) and HGD within 10 to 14 weeks after doxycycline treatment (Figure 1A). These mice first developed pyloric metaplasia, consisting of distinct cell types, including spasmolytic polypeptide expressing metaplasia (SPEM) cells, positive for cluster of differentiation 44 variant 9 (CD44v9) and aquaporin-5, at the base of glands (Figure 1E) and foveolar cells above the SPEM cell zone (Supplementary Figure 1B and D). The pyloric metaplasia gradually progressed to intestinal-type metaplasia and dysplasia.

Trefoil factor 3 (TFF3) was usually expressed in the luminal cells of intestinal-type metaplastic glands.[24,25] The TFF3 expression was significantly increased in the glands with

SPEM cells at the base at 5 to 6 weeks, which is a typical gland composition of incomplete intestinal metaplasia (In-IM)[26] (Figure 1E–H). These In-IM glands progressed to LGD or even HGD in ~25% of the mucosa at 10 to 14 weeks (Figure 1A–C). The HGD displayed cytologic features of dysplastic glands, including loss of cell polarity, increased mitosis, pseudo-stratification, and prominent nucleoli, all features commonly seen in human patients (Figure 1B). Additionally, gland width in Kras-induced stomachs was increased between metaplasia and dysplastic stages (Figure 1D).

Although the number of TFF3-positive IM cells was dramatically decreased in HGD glands (Figure 1G and H), SPEM cells were still present at the base with a decreased coexpression of CD44v9 and aquaporin-5 (Figure 1E and F). The LGD glands exhibited a transitioning cell zone coinciding with cell lineage conversion from metaplastic to trophoblast cell surface antigen 2 (TROP2)-positive dysplastic cells[27] above the SPEM cell zone (Figure 1I and J and Supplementary Figure 1C).

We also observed the expression of 2 additional markers in the apical membranes of dysplastic cells in HGD: CD133, a marker of dysplastic stem cells that contribute to adenocarcinoma development,[13] and carcinoembryonic antigen-related cell adhesion molecule 5 (CEACAM5), a dysplasia and gastric adenocarcinoma marker in human[28,29] (Figure 1K and L and Supplementary Figure 1E, arrowheads). Also, the cell proliferation zone and level were expanded throughout the glands in HGD (Figure 1M and N and Supplementary Figure 1F) and aligned with a distribution of CEACAM5-positive dysplastic cells. We additionally observed that claudin 3, a major structural molecule of tight junctions, was substantially decreased at the very base of LGD and HGD, suggesting the loss of cell polarity and architectural changes in dysplastic glands by modifying tight junction structures (Figure 1O and P). Therefore, these data demonstrate that Kras activation only in chief cells is sufficient to drive the carcinogenic process to HGD with dynamic changes in cell lineage evolution as well as architectural changes in gland structures.

Metabolic Reprogramming Turns on Fatty Acid Metabolism During Metaplasia Progression to Dysplasia

To identify metabolic pathways involved in the carcinogenic process, we performed MALDI-IMS using the GCK stomach tissues[30] (Figure 2A). A series of mass spectra (200–1400 m/z) for metabolites were collected over the tissue area (Supplementary Figure 2A). We profiled ~300 key metabolites associated with major metabolic pathways, including glycolysis and FA, phospholipid, and glutathione metabolism. We then selected metabolites abundant in the metaplastic or dysplastic stages, or both, through in situ visualization of spatial distribution and relative quantitation (Figure 2B and Supplementary Figure 2B–F). Hexose bisphosphates, glycolytic pathway-associated metabolites, were initially elevated in stomachs with pyloric metaplasia and gradually decreased during metaplasia progression (Figure 2B–D). In contrast, long-chain FAs were differentially accumulated during metaplasia progression.

Palmitate is the most common saturated FA, among long-chain FAs, in the human body.[31] Although the palmitate was abundant in normal stomachs, the level was significantly decreased in pyloric metaplasia and then increased in both In-IM and HGD (Figure 2E

and H). In particular, one unique form of monounsaturated FA (MUFA; free FA [FFA] 20:1) (Figure 2G) showed a gradual increase during metaplasia progression and accumulated strongly in HGD (Figure 2F and H). Furthermore, the accumulation of this metabolite was most prominent at the base of glands where dysplastic cell lineage conversion occurs (Figure 2H). It is important to note that oleate (18:1), a well-known form of MUFA produced from palmitate, was also abundant in the stomachs (Figure 2H). However, there was no correlation between oleate accumulation and metaplasia progression.

One polyunsaturated FA (PUFA, FFA 22:4) also displayed a similar accumulation pattern to the MUFA (FFA 20:1) (Supplementary Figure 2B). However, this PUFA (FFA 22:4) uses linoleate as a precursor, which is obtained only from the diet. Therefore, these results revealed that metabolic reprogramming from glycolysis to FA metabolism occurs during metaplasia progression to dysplasia and produces a unique form of MUFA (FFA 20:1).

Stearoyl-Coenzyme A Desaturase–Dependent Fatty Acid Desaturation Is Required for Dysplastic Cell Survival

Because we observed changes in concentration and distribution of key metabolites in dysplastic glands, we examined expression levels of metabolic enzymes important for glycolysis or FA metabolism by using gastric organoids established from each stage of GCK mouse carcinogenesis (Figure 3A and Supplementary Figure 3A–C). Genes associated with glycolysis were highly expressed in In-IM organoids compared with pyloric metaplasia, LGD or HGD organoids. In contrast, expression of genes associated with FA desaturation, including *Scd1*, were increased in LGD and HGD organoids (Figure 3B and Supplementary Figure 3D).

Stearoyl–coenzyme A desaturase (SCD) is a rate-limiting enzyme that produces MUFAs.[32] The SCD1 protein was prominently expressed in the transitioning cell zone in both LGD and HGD, often in cells copositive for Ki-67, a cell proliferation marker (Figure 3C and D and Supplementary Figure 3E).

We next targeted key steps of metabolic pathways in dysplastic organoids that expressed SCD1 (Figure 3E and Supplementary Figure 3F). We treated dysplastic organoids for 3 days with small-molecule inhibitors that target glycolysis or FA metabolism. Inhibition of glycolysis did not affect organoid viability or growth, except for 2-deoxy-D-glucose (2-DG) treatment, which inhibits the first step of glycolysis (Figure 3F and G and Supplementary Figure 3G and H). However, normal gastric organoids also died within 3 days after 2-DG treatment (Supplementary Figure 3I). Inhibiting the first step of glycolysis can cause harsh conditions for the cells, because glucose can be converted to other types of metabolites. Moreover, 2-DG has toxic effects due to its ability to induce endoplasmic reticulum stress and to block protein glycosylation.[33] Thus, this result indicates that the response to 2-DG inhibition was not dysplastic cell-specific.

Inhibition of the pentose phosphate pathway and glutamine metabolism reduced organoid growth only, compared with organoids treated with dimethyl sulfoxide (Figure 3F and G). Inhibition of de novo lipid synthesis and elongation, by targeting adenosine 5’-triphosphate citrate lyase, FA synthase, or elongation of very long-chain FAs protein (ELOVL) activity,

did not show any significant changes in organoids (Figure 3H and I and Supplementary Figure 3J and K). However, inhibition of FA desaturation only by targeting the SCD activity resulted in 100% organoid death (Figure 3H and I and Supplementary Figure 3L–N).

The inhibition of SCD activity using A939572 at 100 nmol/L rapidly impeded organoid growth and survival within 1 day, and only a few SCD1-expressing cells remained, but those cells were negative for Ki-67 (Figures 3J, 4A and B, and Supplementary Figure 3L). Organoids treated with A939572 showed an accumulation of cleaved caspase-3–positive apoptotic cells in the central lumen and a decrease in cell proliferation (Figure 4C). However, normal gastric organoids did not show any significant changes in response to A939572 treatment (Figure 4D–F). Furthermore, SCD inhibition specifically targeted dysplastic cells in vivo. We treated GCK mice with A939572 for 2 weeks at 6 weeks after doxycycline induction (Supplementary Figure 4A) and observed a dramatic change in the gastric mucosa (Figure 4G and Supplementary Figure 4B–D).

The GCK mice treated with vehicle showed metaplasia progression to LGD containing SPEM and transitioning cell zones as well as IM cells. In contrast, H&E staining in the GCK mice treated with A939572 revealed many dying or dead cells in the transitioning and surface areas of glands. The dying or dead cells were negative for both TFF3 and TROP2 (Supplementary Figure 4B). SCD1-positive cells were rarely found in the transitioning area, and those cells were in the process of extrusion from glands (Supplementary Figure 4D).

Although the total number of Ki-67–positive cells per gland did not change (Supplementary Figure 4C), many Ki-67–positive cells were present in the gland lumens, and the nuclei of those Ki-67–positive cells were compressed or fragmented, consistent with an early apoptotic change in proliferating cells[34] (Supplementary Figure 4D, arrowheads). The cell death was confirmed by both cleaved caspase-3 and terminal deoxynucleotidyl transferase–mediated deoxyuridine triphosphate nick-end labeling (TUNEL) (Figure 4H–K, arrowheads). However, SPEM cells were still present at the gland base and not copositive for TUNEL signal (Figure 4J).

We additionally observed that $F4/80^{+}CD68^{-}$ macrophage infiltration was significantly increased in the transitioning and surface zones, indicating an increase in phagocytic activity in the mucosa (Supplementary Figure 4E and F). $F4/80^{+}CD68^{+}$ macrophages, which promote metaplasia progression,[35] were slightly increased only at the base of glands (Supplementary Figure 4G and H). Additionally, we did not observe any noticeable changes in major organs, including the liver, spleen, kidney, and lung, in wild-type mice treated with A939572 (Supplementary Figure 4I). Therefore, these results indicate that SCD-dependent FA desaturation is required for dysplastic cell proliferation and survival.

Stearoyl-Coenzyme A Desaturase–Dependent Fatty Acid Desaturation Produces an Unsaturated Long-Chain Fatty Acid That Fuels Dysplastic Cells

To determine how the unsaturated long-chain MUFAs are used in dysplastic cells, we selected 2 metabolites, EA (20:1, n-9, MUFA) and DA (22:4, n-6, PUFA) (Figure 5A) based on the enhancement of ions detected from IMS (Figure 2H and Supplementary Figure 2B). We cotreated dysplastic organoids with A939572, in combination with EA or DA, for

3 days. Organoids cotreated with A939572 and EA recovered from SCD inhibition and retained organoid growth and spheroidal structures. In contrast, organoids cotreated with A939572 and DA did not show any differences compared with the organoids treated only with A939572 (Figure 5B–D and Video 1). Moreover, dysplastic organoids did not grow and form organoid spheres when the *Scd1* gene was silenced. However, EA supplementation reestablished the phenotypes even though the *Scd1* gene silencing was still maintained (Figure 5E and Supplementary Figure 5A–C).

To determine the subcellular localization of EA in dysplastic cells, we conjugated EA with nitrobenzoxadiazole (NBD), a green-fluorescent compound (NBD-EA) (Figure 5F and Supplementary Figure 5D and E). NBD-EA was not detectable in 2-dimensional monolayer culture of dysplastic cells at 6 hours after treatment, but the fluorescent signal strongly accumulated in mitochondria at 24 hours and was weakly maintained until 48 hours (Figure 5G).

Because EA is imported into mitochondria, we further examined whether EA undergoes FA oxidation, which occurs through mitochondrial aerobic metabolism and produces energy substrate for the trichloroacetic acid cycle.[36] Carnitine palmitoyltransferase (CPT) shuttles long-chain FAs into the mitochondria, and the expression of *Cpt1a*, an isoform of CPT1, was up-regulated in dysplastic organoids (Figure 5H). The organoids cotreated with A939572, EA, and perhexiline, a mitochondrial FA oxidation inhibitor, did not display any significant increase in organoid growth (Figure 5I–K and Video 2), indicating that inhibition of FA oxidation abolished rescue effects of EA in dysplastic organoids. Thus, these data suggest that dysplastic cells use EA as a major substrate for energy production in mitochondria.

Metabolic Rewiring Pattern Is Observed Across Precancerous Lesions in Gastrointestinal Cancers

Epithelial cells in other gastrointestinal tract organs also undergo a sequential progression of carcinogenesis.[37,38] We therefore investigated up-regulation of SCD as an indicator of SCD-dependent FA desaturation during progression of precancerous stages to cancer across the human gastrointestinal tract. We immunostained for SCD in multiple sets of gastrointestinal patient tissue microarrays and sections composed of precancerous lesions and cancers from the stomach, esophagus, and pancreas (Figure 6). In gastric cancer tissues, SCD expression was significantly increased in IM and dysplastic lesions, both LGD and HGD compared with matched pairs of normal (Figure 6A).

Also, SCD was mostly expressed in CD44v9^{-}/TROP2^{+} dysplastic cells, but was also observed in CD44v9^{+}/TROP2^{+} transitioning cells, indicating that SCD prominently increased in the transition area between metaplasia and dysplasia (Figure 6B and Supplementary Figure 6A). SCD was highly expressed in intestinal-type gastric cancer, which develops within a carcinogenic cascade,[39] compared with diffuse-type gastric cancer (Figure 6A and C). In pancreatic cancer, 3 predominant types, including mucinous cystic neoplasia, intraductal papillary mucinous neoplasia, and pancreatic intraepithelial neoplasia, are defined as precancerous lesions.[40] SCD expression was elevated in HGD of all 3 precancerous lesions and adenocarcinoma compared with normal or LGD lesions (Figure 6D and E).

Lastly, esophageal adenocarcinoma develops from precancerous metaplasia, known as Barrett's epithelia, and dysplasia.[41] The SCD expression was significantly increased in esophageal Barrett's epithelia, dysplasia, and adenocarcinoma compared with matched pairs of normal (Figure 6F and G). Therefore, these results indicate that SCD up-regulation is a common feature observed during the precancerous metaplasia progression to dysplasia in the gastrointestinal tract.

To assess whether the SCD-dependent FA desaturation is necessary for human dysplastic cell survival, we treated 9 human gastric organoid lines, derived from patient samples with metaplasia or dysplasia,[23] with A939572. Organoids exhibited a broad spectrum of sensitivity to SCD inhibition (Figure 6H–K and Supplementary Figure 6B–I). Dysplastic organoid lines, which expressed both SCD and TROP2,[13,22] did not grow and died within 6 days after the treatment (Figure 6H–J and L). However, the organoids that expressed SCD weakly and were negative for TROP2 did not respond to treatment (Figure 6H, K, L). These results collectively indicate that SCD function is important for dysplastic cell survival and that SCD-dependent FA desaturation might be activated during the carcinogenic transition from precancerous metaplasia.

Discussion

In this study, we focused on cellular changes in dysplasia induced by Kras activation in zymogen-secreting chief cells in the GCK mouse stomachs. Kras activation generally induces precancerous metaplasia in other gastrointestinal tract organs, and activation of additional oncogenic genes is necessary for progression of the precancerous lesions to malignant stages.[10–12,42–44] In contrast, Kras activation in the GCK mice was sufficient to develop HGD through precancerous metaplasia progression. Histologic phenotypes of GCK stomachs faithfully recapitulated metaplastic and dysplastic gland structures seen in human patients. Continuous cell lineage conversion above the SPEM cell zone denoted a main event of carcinogenic transformation of precancerous cells and distinguished the transitioning cell zone with dysplastic cells. Also, an expansion of proliferating cells and changes in cell adhesion and tight junction molecules, such as CEACAM5 and claudin 3, demonstrated loss of cell polarity and asymmetric cell division that are key architectural and cytologic features indicating progression of metaplasia to dysplasia.

Metabolic processes in cancer cells are heterogeneous.[45] Cancer cells generally use aerobic glycolysis, called the Warburg effect, but aberrantly activated lipid metabolism through increased lipogenesis can also fuel cancer cell proliferation.[46–48] IMS allowed us to distinguish various types of metabolites present in gastric mucosa with different carcinogenic stages. Whereas glycolytic metabolites were abundant in metaplastic glands, FA metabolites were concentrated in dysplastic glands. In particular, high concentrations of a long-chain MUFA, EA (20:1, n-9), was observed in the transitioning cell zone of dysplastic glands, suggesting metabolic rewiring from glycolysis to FA metabolism during metaplasia progression. FAs can be desaturated by different enzymes such as the SCDs and the FA desaturases in mammals.[49]

SCD can control stemness in cancer stem cells, cancer cell proliferation, and even acquired resistance to chemotherapy.[50–52] We observed a distinct pattern of SCD up-regulation during metaplasia progression to dysplasia in the GCK mouse stomachs and in human dysplasia and adenocarcinoma across gastrointestinal tract organs. Inhibition of SCD activity using A939572 specifically targeted dysplastic cells in GCK mice and affected dysplastic organoid growth and survival. However, EA, which can be produced by SCD function, could rescue dysplastic organoids from the inhibition effect on SCD activity, suggesting that SCD-dependent FA desaturation is critical for dysplastic cell proliferation and survival. A synthesized fluorescence-conjugated EA in dysplastic cells revealed that EA can be translocated into the mitochondria, suggesting that the EA might be used as a substrate of FA oxidation to produce high-yield energy in cells.

It is important to note that inhibition of glycolysis did not affect dysplastic cell viability or growth. These findings strongly indicate that use of FA, rather than glucose, as a major energy source is a unique metabolic feature of dysplastic cells, and therefore, EA production might be a surrogate marker of metabolic rewiring in dysplastic cells. Mammalian cells can use 2 major sources of FFAs through de novo lipid synthesis or exogenous FFAs. However, how dysplastic cells generate the EA is not yet clear. Thus, further studies are needed to evaluate the mechanisms of FFA influx into the dysplastic cells and its relative contributions to generating long-chain FAs. Also, ELOVLs are potential candidates, which can add carbon chains up to 20 to produce long-chain FAs.[49] Nevertheless, no significant effects on viability or growth in dysplastic organoids were observed after inhibition of ELOVL1 or ELOVL6 (Supplementary Figure 3J and K), and further studies are required to elucidate specific functions of FA elongation steps in dysplastic cells.

Conclusion

In summary, our study confirms that Kras activation in chief cells is sufficient for the full process of carcinogenesis to HGD in the stomach.[9] Unlike cancer cells, which display diverse cell populations with distinct molecular and metabolic signatures, characteristics of dysplastic cells are relatively simple. SCD up-regulation leads to metabolic rewiring during metaplasia progression to dysplasia. Also, EA can be produced through SCD-dependent FA desaturation and fuels hyperproliferation and survival in dysplastic cells. Therefore, SCD-dependent FA desaturation is an essential adaptation in oncogenic FA metabolism for high energy demand in epithelial carcinogenesis.

Supplementary Material

Refer to Web version on PubMed Central for supplementary material.

Funding

This work was supported by National Institutes of Health (NIH) National Cancer Institute (NCI) grants R37 CA244970 and R01 CA272687 and Vanderbilt-Ingram Cancer Center GI SPORE (P50 CA236733), the AGA Research Foundation's AGA-R. Robert & Sally Funderburg Research Award in Gastric Cancer (AGA2022-32-01), and the Gastric Cancer Foundation (to Eunyoung Choi). Nikki Mitchell Foundation and Pancreas Club Seed Grant, Vanderbilt Supporting Careers in Research for Interventional Physicians and Surgeons (SCRIPS) Faculty Research Award (VUMC66796 [1018894] to Marcus C.B. Tan). The Translational Pathology Shared Resource is supported by NCI Cancer Center Support Grant (5P30 CA68485-19). Core Services were performed through

Vanderbilt University Medical Center's Digestive Disease Research Center National Institute of Diabetes and Digestive and Kidney Diseases grant (P30 DK058404) and Vanderbilt Ingram Cancer Center NCI grant (P30 CA068485), with imaging in the Vanderbilt Digital Histology Shared supported by a VA Shared Instrumentation grant (1IS1BX003097). Esophagus tissue samples were provided by the NCI Cooperative Human Tissue Network (CHTN) supported by NCI (UM1 CA183727). Other investigators may have received specimens from the same tissue specimens. The establishment of tissue array sets was supported by the National Research Foundation of Korea (NRF) grant funded by the Korea government (MSIT, 2021R1C1C1011172) (to Bogun Jang).

Data Availability

The data, analytical methods, and study materials will be made available to other researchers.

Abbreviations used in this paper:

2-DG	2-deoxy-D-glucose
AQP5	aquaporin-5
CD	cluster of differentiation
CD44v9	cluster of differentiation 44 variant 9
CEACAM5	carcinoembryonic antigen-related cell adhesion molecule 5
CPT	carnitine palmitoyltransferase
DA	docosatetraenoic acid
EA	Eicosenoic acid
ELOVL	elongation of very long-chain fatty acids protein
FA	fatty acid
FFA	free fatty acid
GCK	*Gif-rtTA;TetO-Cre;Kras*^{G12D}
HGD	high-grade dysplasia
IMS	imaging mass spectrometry
In-IM	incomplete intestinal metaplasia
LGD	low-grade dysplasia
MALDI	matrix-assisted laser desorption/ionization
MUFA	monounsaturated fatty acid
m/z	mass-to-charge
NBD	nitrobenzoxadiazole
PM	pyloric metaplasia

PUFA	polyunsaturated fatty acid
SCD	stearoyl-coenzyme A desaturase
SPEM	spasmolytic polypeptide expressing metaplasia
TFF3	trefoil factor 3
TROP2	trophoblast cell surface antigen 2
TUNEL	terminal deoxynucleotidyl transferase–mediated deoxyuridine triphosphate nick end labeling

References

1. Arnold M, Abnet CC, Neale RE, et al. Global burden of 5 major types of gastrointestinal cancer. Gastroenterology 2020;159:335–349.e15. [PubMed: 32247694]
2. Hanahan D. Hallmarks of cancer: new dimensions. Cancer Discov 2022;12:31–46. [PubMed: 35022204]
3. Vineis P, Schatzkin A, Potter JD. Models of carcinogenesis: an overview. Carcinogenesis 2010; 31:1703–1709. [PubMed: 20430846]
4. Gillies RJ, Verduzco D, Gatenby RA. Evolutionary dynamics of carcinogenesis and why targeted therapy does not work. Nat Rev Cancer 2012;12:487–493. [PubMed: 22695393]
5. Nam KT, Lee HJ, Sousa JF, et al. Mature chief cells are cryptic progenitors for metaplasia in the stomach. Gastroenterology 2010;139:2028–2037.e9. [PubMed: 20854822]
6. Burclaff J, Willet SG, Saenz JB, et al. Proliferation and differentiation of gastric mucous neck and chief cells during homeostasis and injury-induced metaplasia. Gastroenterology 2020;158:598–609.e5. [PubMed: 31589873]
7. Caldwell B, Meyer AR, Weis JA, et al. Chief cell plasticity is the origin of metaplasia following acute injury in the stomach mucosa. Gut 2022;71:1068–1077. [PubMed: 34497145]
8. Goldenring JR, Mills JC. Cellular plasticity, reprogramming, and regeneration: metaplasia in the stomach and beyond. Gastroenterology 2022;162:415–430. [PubMed: 34728185]
9. Choi E, Hendley AM, Bailey JM, et al. Expression of activated Ras in gastric chief cells of mice leads to the full spectrum of metaplastic lineage transitions. Gastroenterology 2016;150:918–930.e13. [PubMed: 26677984]
10. Douchi D, Yamamura A, Matsuo J, et al. Induction of gastric cancer by successive oncogenic activation in the corpus. Gastroenterology 2021;161:1907–1923.e26. [PubMed: 34391772]
11. Seidlitz T, Chen YT, Uhlemann H, et al. Mouse models of human gastric cancer subtypes with stomach-specific CreERT2-mediated pathway alterations. Gastroenterology 2019;157:1599–1614.e2. [PubMed: 31585123]
12. Fatehullah A, Terakado Y, Sagiraju S, et al. A tumour-resident Lgr5(+) stem-cell-like pool drives the establishment and progression of advanced gastric cancers. Nat Cell Biol 2021;23:1299–1313. [PubMed: 34857912]
13. Min J, Zhang C, Bliton RJ, et al. Dysplastic stem cell plasticity functions as a driving force for neoplastic transformation of precancerous gastric mucosa. Gastroenterology 2022;163:875–890. [PubMed: 35700772]
14. de Vries AC, van Grieken NC, Looman CW, et al. Gastric cancer risk in patients with premalignant gastric lesions: a nationwide cohort study in the Netherlands. Gastroenterology 2008;134:945–952. [PubMed: 18395075]
15. Li X, Egervari G, Wang Y, et al. Regulation of chromatin and gene expression by metabolic enzymes and metabolites. Nat Rev Mol Cell Biol 2018;19:563–578. [PubMed: 29930302]
16. Capolupo L, Khven I, Lederer AR, et al. Sphingolipids control dermal fibroblast heterogeneity. Science 2022; 376:eabh1623.

17. Dmitrieva-Posocco O, Wong AC, Lundgren P, et al. β-Hydroxybutyrate suppresses colorectal cancer. Nature 2022;605:160–165. [PubMed: 35477756]
18. Notarangelo G, Spinelli JB, Perez EM, et al. Oncometabolite d-2HG alters T cell metabolism to impair CD8(+) T cell function. Science 2022;377:1519–1529. [PubMed: 36173860]
19. Martin-Perez M, Urdiroz-Urricelqui U, Bigas C, et al. The role of lipids in cancer progression and metastasis. Cell Metab 2022;34:1675–1699. [PubMed: 36261043]
20. Zaidi N, Lupien L, Kuemmerle NB, et al. Lipogenesis and lipolysis: the pathways exploited by the cancer cells to acquire fatty acids. Prog Lipid Res 2013; 52:585–589. [PubMed: 24001676]
21. Feng WW, Kurokawa M. Lipid metabolic reprogramming as an emerging mechanism of resistance to kinase inhibitors in breast cancer. Cancer Drug Resist 2020; 3:1–17. [PubMed: 32226926]
22. Min J, Vega PN, Engevik AC, et al. Heterogeneity and dynamics of active Kras-induced dysplastic lineages from mouse corpus stomach. Nat Commun 2019;10:5549. [PubMed: 31804471]
23. Kim H, Jang B, Zhang C, et al. Targeting stem cells and dysplastic features with dual MEK/ERK and STAT3 suppression in gastric carcinogenesis. Gastroenterology 2024; 166:117–131. [PubMed: 37802423]
24. Aihara E, Engevik KA, Montrose MH. Trefoil factor peptides and gastrointestinal function. Annu Rev Physiol 2017; 79:357–380. [PubMed: 27992733]
25. Meyer AR, Goldenring JR. Injury, repair, inflammation and metaplasia in the stomach. J Physiol 2018; 596:3861–3867. [PubMed: 29427515]
26. Lee SH, Jang B, Min J, et al. Up-regulation of aquaporin 5 defines spasmolytic polypeptide-expressing metaplasia and progression to incomplete intestinal metaplasia. Cell Mol Gastroenterol Hepatol 2022;13:199–217. [PubMed: 34455107]
27. Riera KM, Jang B, Min J, et al. Trop2 is upregulated in the transition to dysplasia in the metaplastic gastric mucosa. J Pathol 2020;251:336–347. [PubMed: 32432338]
28. Toh J, Hoppe MM, Thakur T, et al. Profiling of gastric cancer cell-surface markers to achieve tumour-normal discrimination. BMJ Open Gastroenterol 2020;7: e000452.
29. Lee SH, Contreras-Panta EW, Gibbs D, et al. Apposition of fibroblasts with metaplastic gastric cells promotes dysplastic transition. Gastroenterology 2023; 165:374–390. [PubMed: 37196797]
30. Stoeckli M, Chaurand P, Hallahan DE, et al. Imaging mass spectrometry: a new technology for the analysis of protein expression in mammalian tissues. Nat Med 2001; 7:493–496. [PubMed: 11283679]
31. Carta G, Murru E, Banni S, et al. Palmitic acid: physiological role, metabolism and nutritional implications. Front Physiol 2017;8:902. [PubMed: 29167646]
32. Paton CM, Ntambi JM. Biochemical and physiological function of stearoyl-CoA desaturase. Am J Physiol Endocrinol Metab 2009;297:E28–E37. [PubMed: 19066317]
33. Laussel C, Leon S. Cellular toxicity of the metabolic inhibitor 2-deoxyglucose and associated resistance mechanisms. Biochem Pharmacol 2020;182:114213.
34. McComb S, Mulligan R, Sad S. Caspase-3 Is transiently activated without cell death during early antigen driven expansion of CD8(+) T Cells in vivo. PLoS One 2010;5: e15328.
35. Petersen CP, Weis VG, Nam KT, et al. Macrophages promote progression of spasmolytic polypeptide-expressing metaplasia after acute loss of parietal cells. Gastroenterology 2014;146:1727–1738.e8. [PubMed: 24534633]
36. Schlaepfer IR, Joshi M. CPT1A-mediated fat oxidation, mechanisms, and therapeutic potential. Endocrinology 2020;161:bqz046.
37. Killcoyne S, Fitzgerald RC. Evolution and progression of Barrett's oesophagus to oesophageal cancer. Nat Rev Cancer 2021;21:731–741. [PubMed: 34545238]
38. Morris JP 4th, Wang SC, Hebrok M. KRAS, Hedgehog, Wnt and the twisted developmental biology of pancreatic ductal adenocarcinoma. Nat Rev Cancer 2010;10:683–695. [PubMed: 20814421]
39. Tan P, Yeoh KG. Genetics and molecular pathogenesis of gastric adenocarcinoma. Gastroenterology 2015;149:1153–1162.e3. [PubMed: 26073375]
40. Matthaei H, Dal Molin M, Maitra A. Identification and analysis of precursors to invasive pancreatic cancer. Methods Mol Biol 2013;980:1–12. [PubMed: 23359146]

41. Weaver JMJ, Ross-Innes CS, Shannon N, et al. .Ordering of mutations in preinvasive disease stages of esophageal carcinogenesis. Nat Genet 2014;46:837–843. [PubMed: 24952744]
42. Aguirre AJ, Bardeesy N, Sinha M, et al. Activated Kras and Ink4a/Arf deficiency cooperate to produce metastatic pancreatic ductal adenocarcinoma. Genes Dev 2003;17:3112–3126. [PubMed: 14681207]
43. Hingorani SR, Wang L, Multani AS, et al. Trp53R172H and KrasG12D cooperate to promote chromosomal instability and widely metastatic pancreatic ductal adenocarcinoma in mice. Cancer Cell 2005;7:469–483. [PubMed: 15894267]
44. Won Y, Choi E. Mouse models of Kras activation in gastric cancer. Exp Mol Med 2022;54:1793–1798. [PubMed: 36369466]
45. Kim J, DeBerardinis RJ. Mechanisms and implications of metabolic heterogeneity in cancer. Cell Metab 2019; 30:434–446. [PubMed: 31484055]
46. Fritz V, Benfodda Z, Rodier G, et al. Abrogation of de novo lipogenesis by stearoyl-CoA desaturase 1 inhibition interferes with oncogenic signaling and blocks prostate cancer progression in mice. Mol Cancer Ther 2010; 9:1740–1754. [PubMed: 20530718]
47. Bansal S, Berk M, Alkhouri N, et al. Stearoyl-CoA desaturase plays an important role in proliferation and chemoresistance in human hepatocellular carcinoma. J Surg Res 2014;186:29–38. [PubMed: 24135379]
48. Snaebjornsson MT, Janaki-Raman S, Schulze A. Greasing the wheels of the cancer machine: the role of lipid metabolism in cancer. Cell Metab 2020;31:62–76. [PubMed: 31813823]
49. Guillou H, Zadravec D, Martin PG, et al. The key roles of elongases and desaturases in mammalian fatty acid metabolism: Insights from transgenic mice. Prog Lipid Res 2010;49:186–199. [PubMed: 20018209]
50. Li J, Condello S, Thomes-Pepin J, et al. Lipid desaturation is a metabolic marker and therapeutic target of ovarian cancer stem cells. Cell Stem Cell 2017;20:303–314.e5002E [PubMed: 28041894]
51. Dai S, Yan Y, Xu Z, et al. SCD1 confers temozolomide resistance to human glioma cells via the Akt/GSK3 β/β-catenin signaling axis. Front Pharmacol 2017;8:960. [PubMed: 29354058]
52. Lien EC, Westermark AM, Zhang Y, et al. Low glycaemic diets alter lipid metabolism to influence tumour growth. Nature 2021;599:302–307. [PubMed: 34671163]

WHAT YOU NEED TO KNOW

BACKGROUND AND CONTEXT

Gastrointestinal cancer commonly develops within a carcinogenic cascade from precancerous metaplasia to dysplasia and adenocarcinoma. Dysplasia is a focal neoplastic lesion and has the highest risk of cancer development.

NEW FINDINGS

Metabolic rewiring from glycolysis to fatty acid metabolism occurs during carcinogenic transition of precancerous metaplasia to dysplasia and is a critical adaptation to fuel dysplastic cell hyperproliferation and survival.

LIMITATIONS

An altered fatty acid metabolic pathway was identified during precancerous metaplasia progression to dysplasia; however, whether gastric cancer cells are also dependent on the altered metabolic pathway is unclear.

CLINICAL RESEARCH RELEVANCE

Although metabolism has become a promising chemotherapeutic target in cancer therapy, which metabolic pathways regulate gastric carcinogenesis remains undefined. The novel insights and clinical implications provided allow targeting the function of stearoyl-coenzyme A desaturase before the gastric adenocarcinoma arises in patients.

BASIC RESEARCH RELEVANCE

Kras activation only in zymogen-secreting chief cells recapitulates the carcinogenic cascade in gastric cancer development seen and develops high-grade dysplasia. Metabolic rewiring from glycolysis to fatty acid metabolism can lead to precancerous metaplasia progression to dysplasia, and the altered fatty acid metabolism is needed for dysplasia cell proliferation and survival.

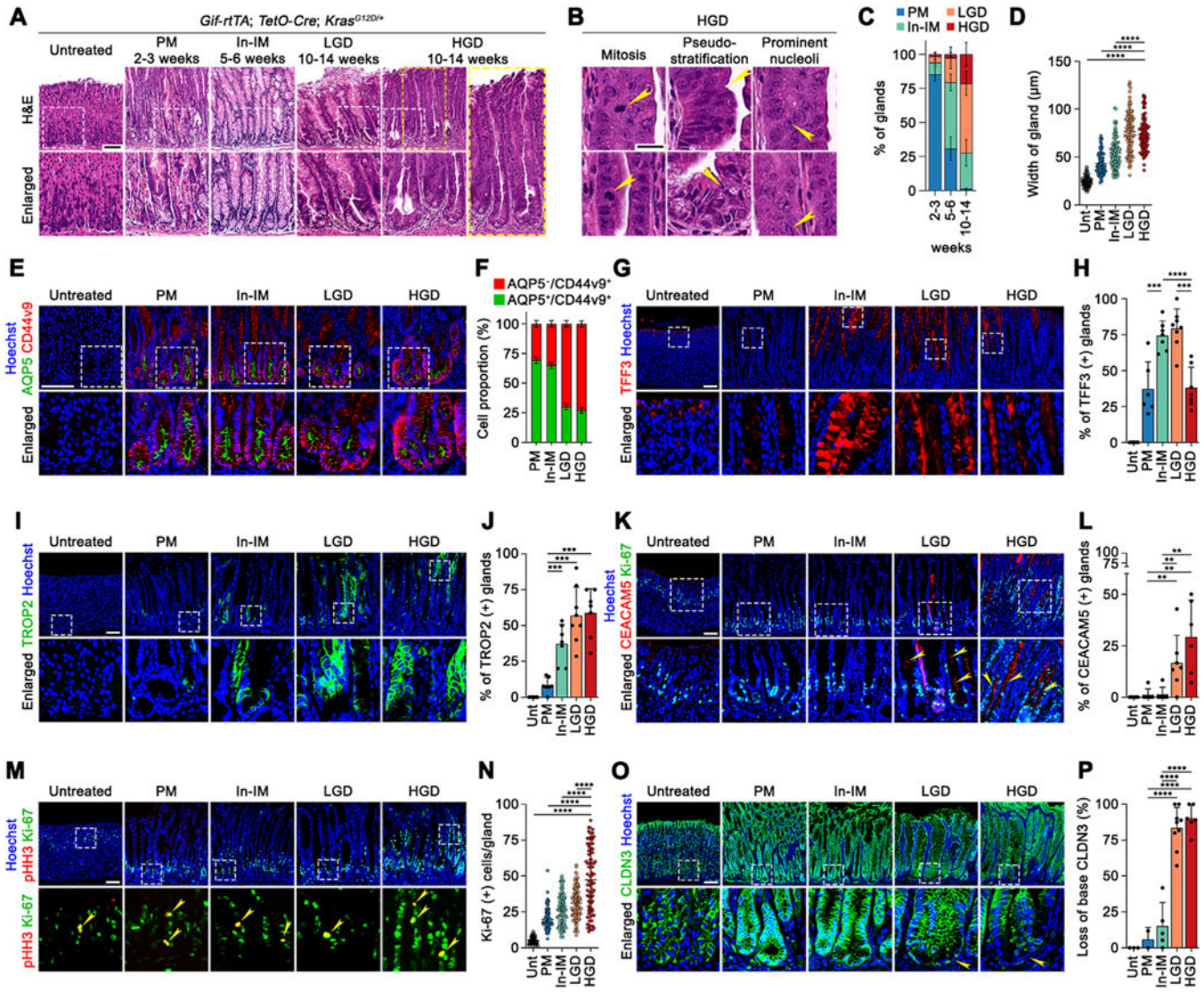

Figure 1.

Key stages of gastric carcinogenesis induced by Kras activation in gastric chief cells. (*A*) H&E-stained images from the GCK mouse stomachs at multiple times after doxycycline treatment: pyloric metaplasia (PM; 2–3 weeks), In-IM (5–6 weeks), and LGD/HGD (10–14 weeks). (*B*) Cytologic features of dysplasia, observed in HGD, are indicated by arrowheads. (*C*) Proportion of gland types in GCK stomachs. We examined 100 glands in the proximal region of the corpus at 2 to 3 weeks (n = 5), 5 to 6 weeks (n = 8), and 10 to 14 weeks (n = 10). (*D*) Measurement of glands width in GCK stomachs. A total of 100 glands were examined in each group, 3 mice per group. Each dot indicates the width of glands. Unt, untreated. (*E*) Immunofluorescent (IF) staining for CD44v9 (red) and aquaporin 5 (AQP5, green) for SPEM cell lineage. (*F*) Quantitation of positive cells for CD44v9 or AQP5, or both. A total of 100 glands were examined in each group, 3 mice per group. (*G*) IF staining for TFF3 (red) for IM cells. (*H*) Quantitation of TFF3-expressing glands. (*I*) IF staining for TROP2 (green). (*J*) Quantitation of TROP2-expressing glands. (*K*) IF staining for CEACAM5 (red; arrowheads) and Ki-67 (green). (*L*) Quantitation of CEACAM5-expressing

glands. Each dot in *H*, *J*, and *L* indicates the percentage of positive glands per 20× field of images. (*M*) IF staining for phospho-histone H3 (pHH3; red) and Ki-67 (green). Arrowheads indicate copositive cells for pHH3 and Ki-67. (*N*) Quantitation of Ki-67–positive cells per gland. Each dot indicates the Ki-67–positive cells per gland. (*O*) IF staining for claudin 3 (CLDN3) (green). (*P*) Quantitation of loss of CLDN3 expression (arrowheads). Each dot indicates the percentage of CLDN3-negative glands per 20× field image. All IF data are representative of n = 3 mice per group, and 100 glands per group were examined for quantitation. Hoechst was used for nuclear staining. The white dotted boxes denote enlarged regions. Scale bars: 25 μm (B) and 100 μm (*A, E, G, I, K, M, and O). D, H, J, L, N*, and *P* show the mean ± standard deviation. C and F show the mean ± standard error of the mean. Two-tailed unpaired t test (*H, J*, and *P*), 2-tailed Mann-Whitney test (*L* and *N*), or Kruskal-Wallis test with 2-sided Dunn's multiple comparison test (*D*). $^{**}P < 0.01$, $^{***}P < 0.001$, $^{****}P < 0.0001$.

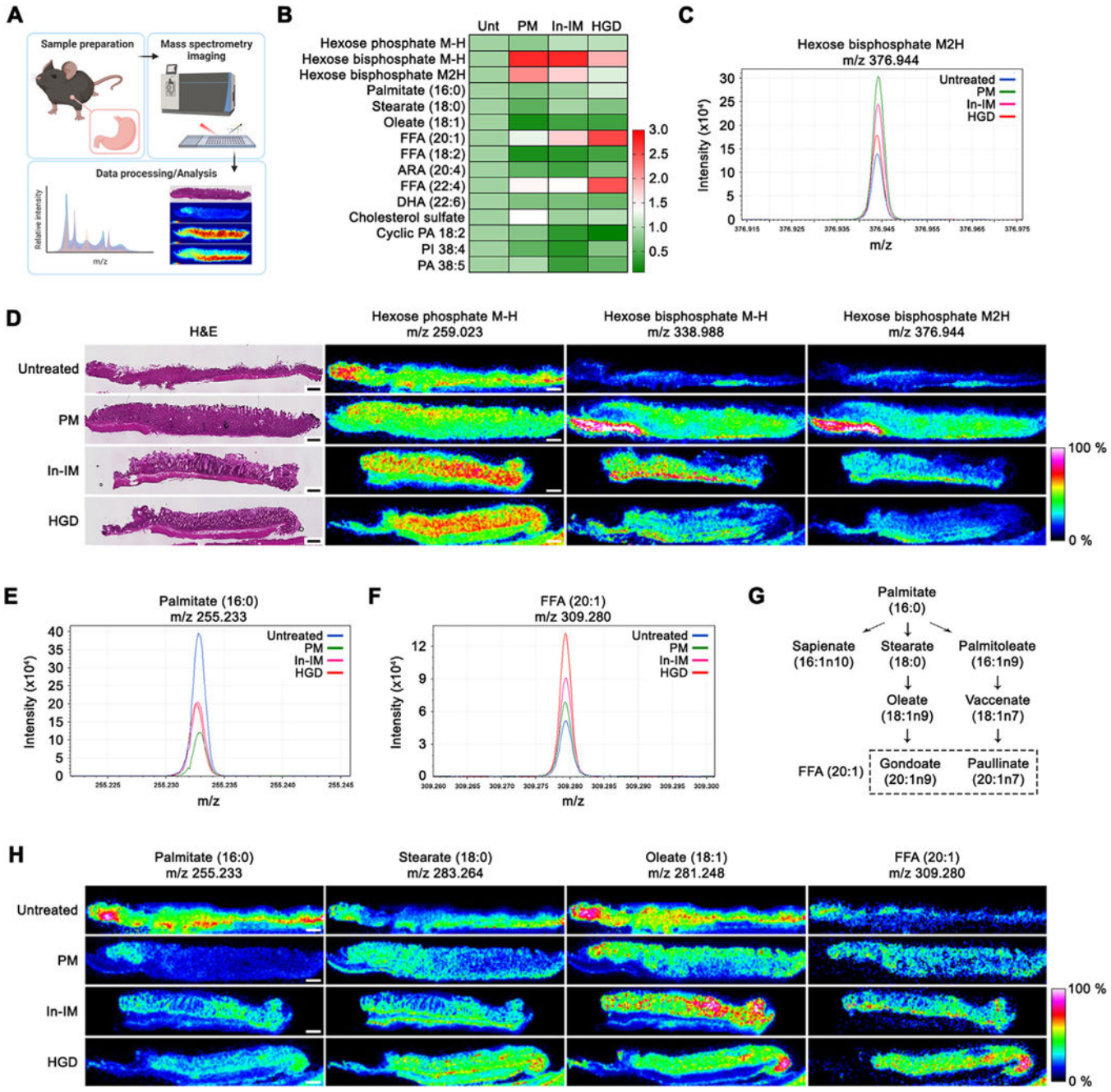

Figure 2.

Spatial and quantitative metabolic profiling reveals distinct patterns of metabolites during carcinogenesis. (*A*) Schematic for methodology of MALDI-IMS using GCK stomachs. The mass spectrum images were obtained per each ion by plotting m/z intensity collected from each spot. (*B*) Heat map displays relative values of average pixel intensity of the individual metabolite at untreated (Unt), pyloric metaplasia (PM), In-IM, and HGD stages. The color box indicates a relative pixel intensity value of total ion counts compared with untreated stomach. ARA, arachidonic acid; DHA, docosahexaenoic acid; PA, phosphatidic acid; PI, phosphatidylinositol. (*C*) An overlay of hexose bisphosphate intensities. (*D*) Ion images

of hexose phosphate and hexose bisphosphates in the GCK stomachs (*left*; H&E staining corresponding to the tissue section used for the IMS). An overlay of (*E*) palmitate or (*F*) MUFA (FFA 20:1) intensities. (*G*) Schematic for FA desaturation and elongation. (H) Ion images of long-chain FAs in the GCK stomachs. The abundance of individual metabolites is normalized to 100%. Scale bar: 500 μm.

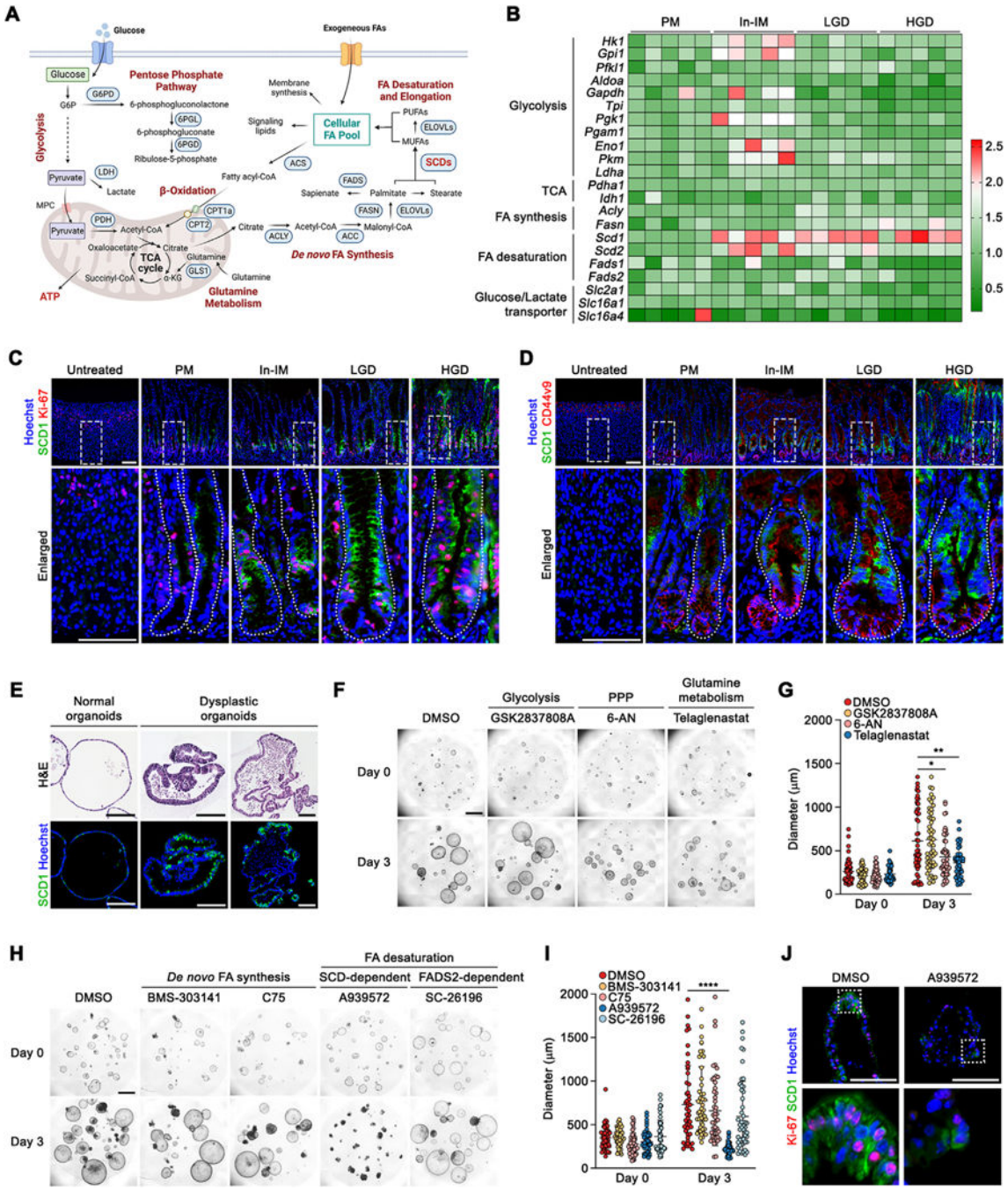

Figure 3.

Specific expression of SCD1 in GCK stomachs. (*A*) Schematic for key steps in central metabolic pathways with associated enzymes. ACLY, adenosine 5'-triphosphate citrate lyase; FADS, FA desaturase; FASN, fatty acid synthase; GLS1, glutaminase; LDH, lactate dehydrogenase; MPC, mitochondrial pyruvate carrier; PDH, pyruvate dehydrogenase; TCA, tricarboxylic acid cycle. (*B*) Heat map displays relative messenger RNA levels of genes encoding metabolic enzymes or transporters in gastric organoid lines derived from GCK stomachs from 5 independent experiments. The color box indicates a relative

expression level of genes normalized to the *Rplp0* at the pyloric metaplasia stage. All individual values are shown in Supplementary Figure 3D. (*C* and *D*) Immunofluorescent (IF) staining for SCD1 (green) and Ki-67 (red) or CD44v9 (red) in GCK stomachs. White dotted boxes denote enlarged regions. White dotted lines identify gland shapes. All IF data are representative images of n = 3 mice per group, and Hoechst was used for nuclear staining. (*E*) IF staining for SCD1 (green) in normal or dysplastic organoids. (*F*) Phase-contrast images of dysplastic organoids treated with dimethyl sulfoxide (DMSO; vehicle), GSK2837808A (LDH inhibitor; 10 μmol/L), 6-aminonicotinamide (6-AN, glucose-6-phosphate dehydrogenase [G6PD] inhibitor; 50 μmol/L), telaglenastat (GLS1 inhibitor; 1 μmol/L) for 3 days. (*G*) Quantitation of organoid diameters in dysplastic organoids treated with inhibitors of glycolysis metabolic enzymes for 3 days. (*H*) Phase-contrast images of dysplastic organoids treated with dimethyl sulfoxide (DMSO) (vehicle), BMS-303141 (ACLY inhibitor; 1 μmol/L), C75 (FASN inhibitor; 1 μmol/L), A939572 (SCD inhibitor; 100 μmol/L), or SC-26196 (FA desaturase [FADS2] inhibitor; 1 μmmol/L) for 3 days. (I) Quantitation of organoid diameters in dysplastic organoids treated with inhibitors of lipid metabolic enzymes for 3 days (n = 50). (*G* and *I*) organoids from 3 independent experiments. (*J*) IF staining for Ki-67 (red) and SCD1 (green) in dysplastic organoids treated with DMSO or A939572 for 1 day. Scale bars: 100 μm (*C, D, E,* and *J*) and 1000 μm (*F* and *H*). All panels show mean ± standard deviation. Two-tailed Mann-Whitney test. * $P < 0.05$, ** $P < 0.01$, **** $P < 0.0001$.

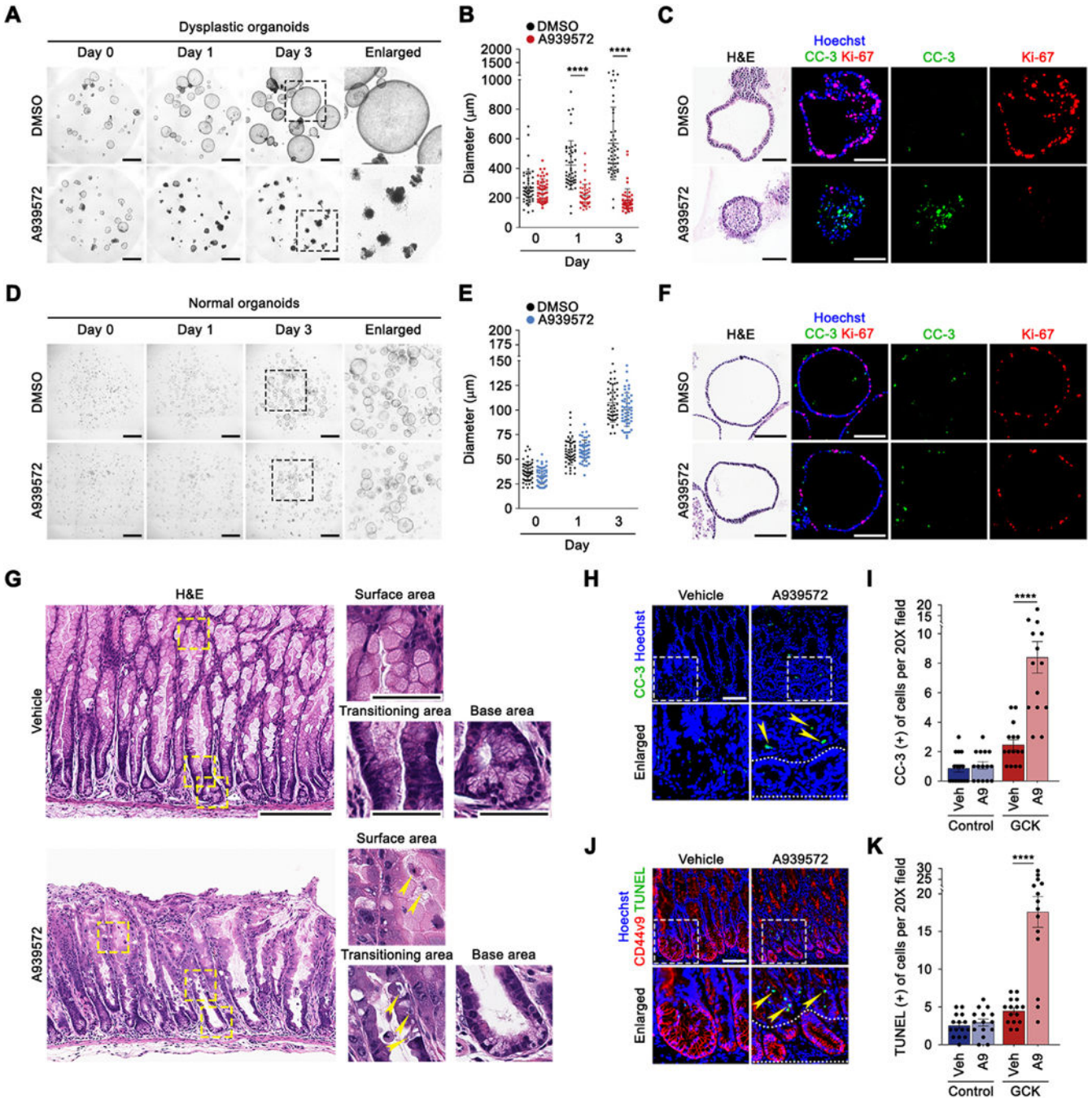

Figure 4.

SCD1 regulates dysplastic cell proliferation and survival both in vivo and in vitro. (*A* and *D*) Phase-contrast images of organoids treated with dimethyl sulfoxide (DMSO; vehicle) or A939572 (100 nmol/L) at 0, 1, or 3 days after treatment. (*B* and *E*) Quantitation of organoid diameters (n = 50 organoids from 3 independent experiments). (*C* and *F*) H&E staining or immunofluorescent (IF) staining for cleaved caspase-3 (CC-3, green) or cell proliferation (Ki-67, red) in organoids treated with either DMSO or A939572 (n ≥ 3 biological replicates). (G) H&E staining in GCK mouse stomachs treated with vehicle (n

= 3) or A939572 (n = 4). Arrowheads indicate dead cells. (H) IF staining for CC-3 (green) in GCK mouse stomachs treated with DMSO (vehicle) or A939572. Arrowheads indicate CC-3–positive cells. (*I*) Quantitation of CC-3–positive cells per 20× field of images. (*J*) IF staining for terminal deoxynucleotidyl transferase–mediated deoxyuridine triphosphate nick-end labeling (TUNEL, green) in the vehicle- or A939572-treated GCK stomachs. Arrowheads indicate TUNEL-positive cells. (*K*) Quantitation of TUNEL-positive cells per 20× field of images. Each dot in *I* and *K* indicates the CC-3–positive or TUNEL-positive cells in each 20× field image. *Scale bars*: 50 μm (G, enlarged), 100 μm (*C, F, H*, and *J*, 200 μm (G, left), and 1000 μm (*A* and *D*). Hoechst was used for nuclear staining. Dotted boxes denote enlarged regions. All panels show mean ± standard deviation. Two-tailed unpaired *t* test (*E* and *K*) or 2-tailed Mann-Whitney test (*B* and *I*). **** $P < 0.0001$.

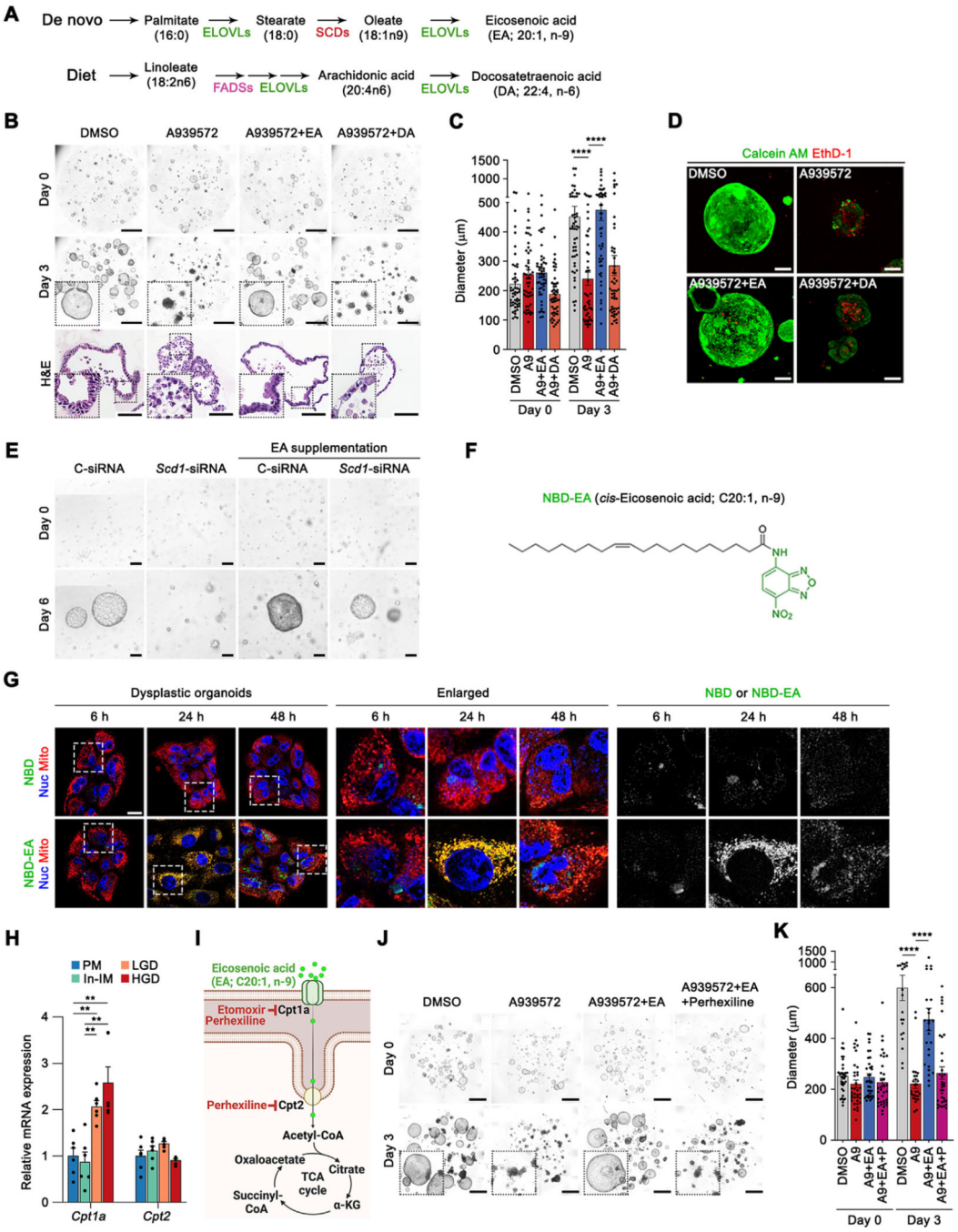

Figure 5.

EA is used a key energy substrate of FA oxidation. (*A*) Schematic for FA elongation and desaturation for EA (20:1, n-9) or DA (22:4, n-6). (B) Phase-contrast, H&E-stained images and (*C*) quantitation of organoid diameters of dysplastic organoids cotreated with A939572, in combination with EA or DA for 3 days (n = 50 organoids from 3 independent experiments). DMSO, dimethyl sulfoxide. (*D*) Live/dead (calcein acetoxymethyl/ethidium homodimer-1 [EthD-1]) cell staining of dysplastic organoids cotreated with A939572, in combination with EA or DA for 3 days. (*E*) Phase-contrast images of dysplastic organoids

treated with *Scd1*-small interfering (si)RNA or control-siRNA (C-siRNA) alone or in combination with EA at day 0 or 6 days after the treatment. (*F*) Chemical structure of synthesized NBD-conjugated EA (20:1, n-9). (*G*) Confocal *images* of dysplastic cell monolayers cultured with NBD or NBD-EA at 6, 24, and 48 hours after incubation. Cells were then stained with 100 nmol/L of MitoTracker Red CMXRos (Mito). Hoechst was used for nuclear staining (Nuc). (*H*) Relative messenger RNA (mRNA) expression levels of *Cpt1a* and *Cpt2* genes in gastric organoid lines (n = 3 independent experiments). (*I*) Schematic for target molecules of perhexiline in the FA oxidation. (*J*) Phase-contrast images and (*K*) quantitation of diameters of dysplastic organoids after the cotreatment (n = 20–35 organoids from 3 independent experiments). Dotted boxes denote enlarged regions. Scale bars: 20 μm (*G*), 100 μm (C; H&E images, *E* and *F*), and 1000 μm (*C*; phase-contrast images and *J*). All panels show mean ± standard deviation. Two-tailed Mann-Whitney test. $^{**}P < 0.01$, $^{****}P < 0.0001$.

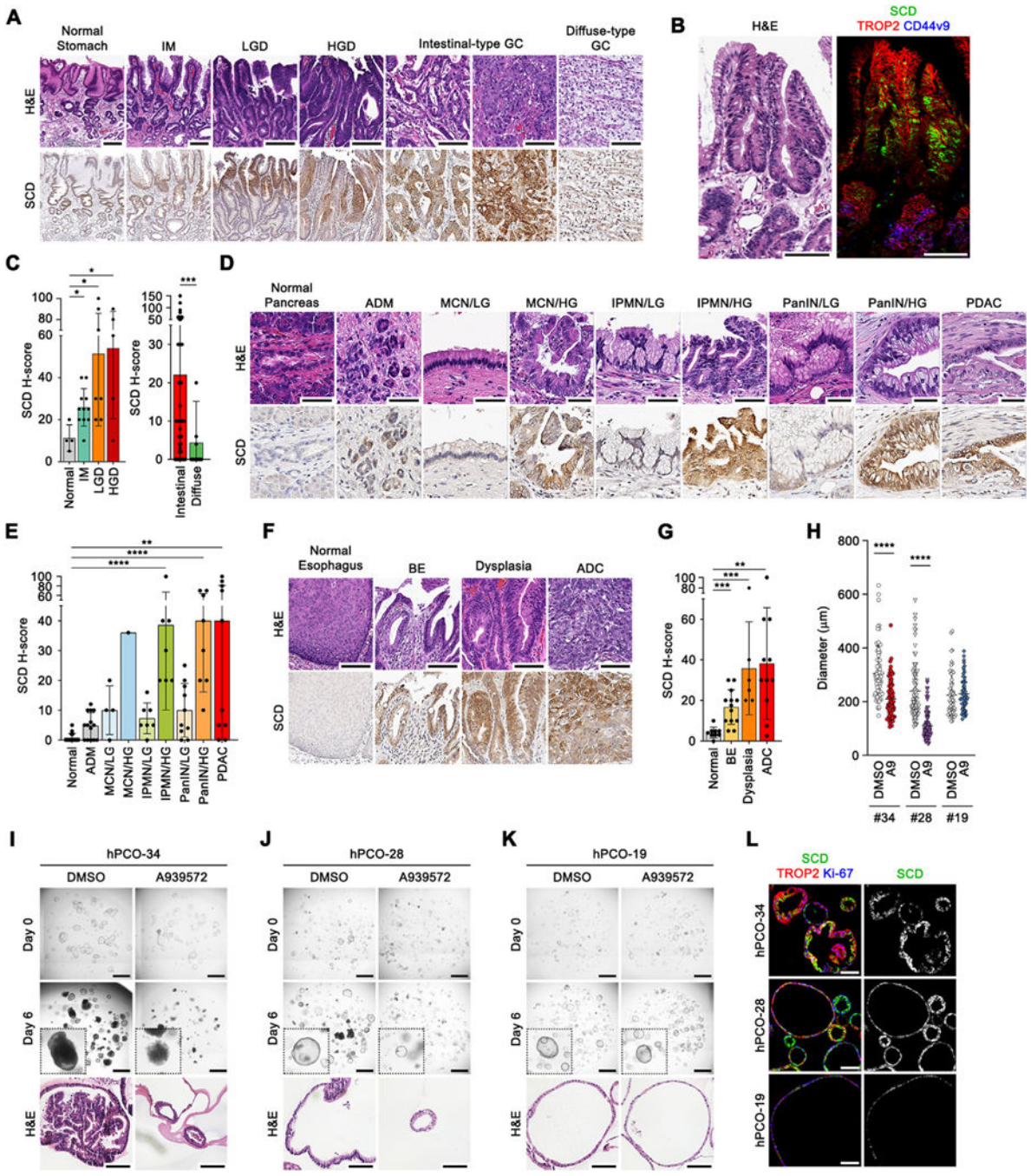

Figure 6.

SCD up-regulation in human gastrointestinal carcinogenesis. (*A*) Immunohistochemistry (IHC) staining for human SCD in adjacent normal ($n = 4$), IM ($n = 11$), LGD ($n = 7$), HGD (n = 5), and intestinal- or diffuse-type gastric cancer (GC) tissues (n = 89). (*B*) Representative images of H&E and coimmunostaining for SCD (green), TROP2 (red), and CD44v9 (blue) in human stomach tissues. (*C*) The IHC H-score of SCD in human stomach tissues. (*D*) IHC staining for SCD in adjacent normal (n = 16), acinar-toductal metaplasia (ADM, n = 14), mucinous cystic neoplasia (MCN, n = 5), intraductal papillary

mucinous neoplasia (IPMN, n = 14), pancreatic intraepithelial neoplasia (PanIN, n = 18), and pancreatic ductal adenocarcinoma (PDAC, n = 10). (*E*) The IHC H-score of SCD in human pancreatic00 tissues. (*F*) IHC staining for SCD in adjacent normal (n = 9), Barrett's esophagus (BE, n = 13), dysplasia (n = 6), and esophageal adenocarcinoma (ADC, n = 11). (*G*) The IHC H-score of SCD in human esophageal tissues. (*H*) Quantitation of diameters of human precancerous organoids (hPCOs) at 6 days after treatment with dimethyl sulfoxide (DMSO) or A939572 (n = 57–84 organoids from 3 independent experiments). (*I–K*) Phase-contrast and H&E-stained images of hPCOs treated with DMSO or A939572 (1 μmol/L). (*I*) High, (*J*) moderate, or (*K*) low response to A939572 treatment. (*L*) Immunofluorescent staining for SCD (green) and TROP2 (red), and Ki-67 (blue) in hPCOs (n ≥ 3 independent experiments for A939572 treatment in hPCOs). *Scale bars*: 50 μm (*A* and *F*), 100 μm (*B, D, L*, and *I–K*; H&E images), and 1000 μm (*I–K*; phase-contrast images). All panels show mean ± standard deviation. Two-tailed unpaired t test (*C*; left), 2-tailed Mann-Whitney test (*C*; right, *E*, and *H*), or Kruskal-Wallis test with 2-sided Dunn's multiple comparison test (*G*). *P < 0.05, **$P < 0.01$, ***$P < 0.001$, ****$P < 0.0001$.